Dalton Transactions

Accepted Manuscript

ROYAL SOCIETY OF CHEMISTRY

www.rsc.org/dalton

Observation of magnetoelectric coupling and local piezoresponse in modified $(Na_{0.5}Bi_{0.5})TiO_3$-$BaTiO_3$-$CoFe_2O_4$ lead-free composites

E.Venkata Ramana[1*], F.Figueiras[2], M.P.F.Graça[1], and M.A.Valente[1]

[1] I3N-Aveiro, Department of Physics, University of Aveiro, Aveiro-3810 193, Portugal.

[2] CICECO, University of Aveiro, Aveiro-3810 193,Portugal.

Lead-free particulate multiferroic composites of $[0.94(Na_{0.5}Bi_{0.5})TiO_3$-$0.06$ $BaTiO_3]$:$(Co_{0.6}Zn_{0.4})(Fe_{1.7}Mn_{0.3})O_4$ were synthesized and magnetoelectric (ME) properties were studied. X-ray diffraction and microstructural studies indicated the formation of two-phase composite system without any impurities. The shift of Raman modes corresponding to ferroelectric and ferrite phases was assigned to the induced strain amid the formation of two-phase system, in relation to the fraction of each phase in the samples. A strong local piezoresponse and hysteresis loops observed for composites established the ferroelectric properties at nanoscale. Magnetostriction measurements revealed values of λ_{11}= -10.4 and λ_{12}=5.3 ppm and piezomagnetic coefficient $d\lambda_{11}/dH$= -0.0087 ppm/Oe at 0.45 kOe for composite with ferrite concentration of 35 mol. %. A maximum change of 18.5 % in magnetization after electrical poling indicates a strong magnetoelectric response of present composites followed by a direct ME coefficient of 8.2 mV/cm-Oe. Our studies points to the fact that the present multiferroic composites having strong ME coupling are useful for lead-free electronic applications.

* Author for correspondence: venkataramanaesk@rediffmail.com

1. Introduction

Multiferroic materials, showing two or more primary ferroic orderings such as ferroelectricity and ferromagnetism simultaneously, have attracted significant research interest due to their potential for cost effective, fast communication and sensor device applications [1,2]. The magnetoelectric (ME) coupling, characterized by electric polarization modulated by a magnetic field (direct ME) or electric field induced magnetic anisotropy (converse ME) offers significant promise for a wide range of applications, in sensors, highly sensitive magnetometers, tunable inductors, nanoscale electromagnet, and magnetic random access memory (MRAM)[2-5]. Room temperature ME effects in single-phase materials are weak. On the contrary, multiferroic composites show stronger strain mediated ME effect due to the interface-related and proximity field effects. In bulk particulate composites, higher piezoelectric and magnetostrictive properties of participating phases have led to giant ME coupling [6-9]. However, most of the studies were focused on composites involving Pb-based ferroelectrics such as $Pb(Zr,Ti)O_3$ (PZT), $PbTiO_3$ (PT), $Pb(Mg,Nb)O_3$ (PMN). In view of environmental hazards, it is necessary to find materials for Pb-free applications.

In recent years there has been considerable interest in the design of lead-free ME composites. Following are some of important observations in lead-free materials: 0.43 mV/cm-Oe was reported in $NiFe_2O_4$-$(Ba_{0.8}Sr_{0.2})TiO_3$ composites[10]; 15.01 mV/cm-Oe was observed for $CoFe_2O_4$-$K_{0.5}Na_{0.5}NbO_3$-$LiSbO_3$[11]; 0.375 mV/cm-Oe was reported in $BaTiO_3$-$(Li,Co)Fe_2O_4$[12]; 0.155 mV/cm-Oe was reported in NBT-$NiFe_2O_4$[13]. Recently, Yang et al.[14] observed a strong ME response with a coefficient of 20.14 mV/cm-Oe for $0.948(K_{0.5}Na_{0.5}NbO_3)$-$0.052LiSbO_3$-$Ni_{0.8}Zn_{0.2}Fe_2O_4$ composites and 261 mV/cm-Oe in laminate fabricated using this composite and Ni.

$1\text{-}x(Na_{0.5}Bi_{0.5})TiO_3\text{-}xBaTiO_3$ (NBBT, x=0.05-0.07) compound, with a rhombohedral-tetragonal morphotropic phase boundary (MPB) has emerged as a potential lead-free material for piezoelectric applications. Single crystalline NBBT exhibits a large piezoelectric coefficient, d_{33}, of 500 pC/N [15] where as random polycrystalline samples show a value of 120-160 pC/N [16,17]. It was reported that after texturing the coefficient enhances up to 322 pC/N [17]. In addition to the piezoelectric properties, its higher ferroelectric-paraelectric temperature (225-228 ^oC) [18] allows this material to be used at higher operating temperatures without depoling. In the present work, we have synthesized particulate ME composites by mixing Zn and Mn doped $CoFe_2O_4$ (CFO) with NBBT.

In ferrites class, undoped CFO exhibits a large magnetostriction (λ) in the range 150-250 ppm [19]. Doping CFO with Mn for Fe ($CoFe_{1.7}Mn_{0.3}O_4$) and Zn for Co ($Co_{0.6}Zn_{0.4}Fe_2O_4$) is reported to reduce magnetic anisotropy constant and coercivity keeping the value of λ comparable to that of CFO [19-21]. Gupta et al. [22] reported a larger enhancement of ME coefficient in Mn and Zn co doped CFO-PZT composites compared to the undoped composite samples. In view of these results, we expect an improved ME coupling in the composites involving NBBT and $Co_{0.6}Zn_{0.4}Fe_{0.7}Mn_{0.3}O_4$ (CZFMO) compounds. We present here ferroelectric, local piezoresponse and ME coupling of the composite samples.

2. Experimental

Ceramic composites of $(Na_{0.5}Bi_{0.5}TiO_3)_{0.94}\text{-}(BaTiO_3)_{0.06}$ (NBBT) and CZFMO were synthesized by the conventional solid state sintering method. High purity (Sigma, 99.9%) starting reagents Na_2CO_3, Bi_2O_3, $BaCO_3$ and TiO_2 were weighed according to the stoichiometry of NBBT and ball milled for 24 h under ethanol. Resulting slurries

were dried and calcined at 850 ^{o}C for 3 h. CZFMO was synthesized separately by milling Co_3O_4, ZnO, Fe_2O_3 and Mn_2O_3 for 24 h under ethanol, drying and calcining at 1100 ^{o}C for 8 h. These two constituent powders after calcination were mixed in molecular ratios (NBBT: CZFMO) 40:60, 65:35, 75:25, 85:15, ground thoroughly and calcined at 1000 ^{o}C for 3h. The resulting powders were milled for 6 h and pelletized under a pressure of 100 MPa. The pellets (7 mm in diameter and ~1 mm thick) were sintered in covered alumina crucibles at 1100 ^{o}C. To prevent possible evaporation of volatile species during sintering process, all the samples were embedded in powders of same composition.

Structural analysis of the sintered ceramics was carried out using the Phillips x-ray diffractometer. For this purpose, sintered discs were crushed into powders and heat treated at 400 ^{o}C to relieve mechanical strains. Surface morphology of the sintered ceramics was observed by the scanning electron microscope (SEM, Hitachi S-4100). Raman spectra were measured using the micro-Raman spectrometer (Horiba Jobin Vyon) with a 633 nm excitation laser, an edge filter for Rayleigh line rejection, and a CCD detector. The overall spectral resolution of the system was ~1 cm^{-1}. The laser was focused on the sample to a spot size of ~2 μm using a 50 x objective lens. Magnetic properties were measured using the vibrating sample magnetometer (Cryogenic VSM). For electrical measurements the sintered circular disc samples were polished and silver paste was applied on both faces of the disc to make electrical contact. The silver paste coated samples were fired at 500 ^{o}C for 1 h to form proper electrodes. Polarization-electric field hysteresis loops were measured using the hysteresis loop tracer TF-Analyzer (aixACCT). Electrical poling was performed in the field range 40-60 kV/cm for 30 min at 80 ^{o}C in silicone oil (Merck) bath and field cooled to room temperature. Piezoelectric charge coefficient (d_{33}) was measured after aging the poled samples (for

24 h) using a piezometer (PM100). The dependence of longitudinal strain (S) on electric field (E) with amplitude of 7 kV/mm was measured at a frequency of 0.1 Hz in a silicone oil bath using a linear variable differential transformer. Local piezoresponse was visualized using a commercial scanning probe microscope (Ntegra Prima, NT-MDT) equipped with an external lock-in amplifier (SR 830, Stanford Research) and a function generator (Yokogawa, FG 120). Magnetostriction measurements were carried out using strain gauges and an electromagnet. Magnetoelectric measurements were done by varying the bias magnetic field (1T) under a superimposed ac magnetic field of 1 Oe (f=1 kHz) generated by Helmholtz coils. The voltage output generated from the composite was measured by the lock-in amplifier (Stanford, SR532); the reference signal was taken from the signal generator feeding the Helmholtz coils.

3. Results and discussion

X-ray diffraction patterns of the NBBT-CZFMO composite ceramics sintered at 1100 ^{o}C are shown in Fig. 1. XRD indicates that both end compounds NBBT and CZFMO are formed in single phase with high crystallinity. All the diffraction peaks can be indexed with reference to the standard X-ray patterns of their parent compounds CFO [23] and NBBT [24] respectively. For NBBT sample, XRD peak splitting was observed around $2\theta=40^{o}$ and 47^{o}. These reflections are assigned to (003)/(021), (002)/(200) splitting of the combined rhombohedral and tetragonal features which are associated with the MPB composition of 94% NBT-6% BTO solid solutions [16]. The lattice parameters, calculated from diffraction patterns for NBBT (a = 3.918Å, α=89.926 ^{o}) and CZFMO (a = 8.428 Å) indicate that these two compounds are crystallized in rhombohedral (MPB) and cubic symmetries respectively. CFO has a cubic structure with a lattice parameter of 8.39 Å. The replacement of Zn^{2+} for Co and Mn^{3+} for Fe resulted in larger cell parameter and volume. XRD patterns of 65:35, 75:25 and 85:15

composites exhibit peaks corresponding to both the ferroelectric and ferrite phases without any impurities, indicating no chemical reaction at the ferrite-ferroelectric interface. The intensity of peaks corresponding to ferrite is higher in the ferrite-rich phases of the composites and vice versa. The compositional dependence of lattice parameters corresponding to NBBT and CZFMO phases of composites is presented in Fig. 2. A systematic increase in a $_{CZFMO}$, corresponding to lattice expansion with the increase in NBBT content, can be seen. At the same time, decreasing trend in the values of a $_{NBBT}$ and α (increase in rhombohedral distortion, 90-α) indicates a compression of unit cell volume with the increase in ferrite content. These changes can be attributed to the compressive stress as a result of lattice mismatch (about 7 %) between NBBT and CZFMO.

Fig. 3 shows the surface morphology of (a) CZFMO, (b) 65:35, (c) 85:15 and (d) NBBT samples. Formation of two phase composite systems can be observed from the images (Fig. 3 c and d). It can be seen that the composites have a dense microstructure with ferrite (smaller) and ferroelectric (larger) grains. The average grain size of parent CZFMO and NBBT are found to be in the range 2-3 μm and 4-5 μm respectively. It was observed that the grain size of NBBT and CZFMO phases in composites is larger compared to their parent compounds shown in Fig. 3 (a) and (d). For the composites one can see a densely packed microstructure with ferrite grains embedded in NBBT matrix forming the 0-3 particulate composites. SEM images confirm that composites have no other additional phases due to inter diffusion between constituent phases as evidenced by XRD. In order to find the composition of each grain, we performed EDS mapping. Fig. 4 shows the composition map for ferroelectric and ferrite grains. As expected the larger grains contain composition of NBBT distributed throughout the grains. The

observation of smaller grains with homogenous distribution of Co, Fe, Mn and Zn indicates the successful formation of CZFMO dispersed into the NBBT matrix.

The formation of two-phase composites and the effect of composition on its structure were further investigated by Raman spectroscopy. Fig. 5 shows the room temperature Raman spectra of NBBT, CZFMO and NBBT-CZFMO composite samples. The vertical lines indicate the Raman modes corresponding to individual phases. The Raman modes are assigned based on the Lorentzian fitting of individual peaks of the spectra of all the samples. The well defined peaks at 167, 294, 471, 612 and 672 cm^{-1} match well with the Raman modes reported in literature [25, 26] for undoped CFO at 188, 300, 471, 617 and 683 cm^{-1}. The departure of the observed modes from their mean position can be attributed to the doping of Zn and Mn at tetrahedral (T) and octahedral sites respectively. Group theory analysis predicted several phonon modes such as $A_{1g}(R)$, $E_g(R)$, T_{1g}, $3T_{2g}(R)$, $2A_{2u}$, $2E_u$, $4T_{1u}$ (IR) and $2T_{2u}$ for cubic CFO with space group O^7_h (Fd3m). Out of these phonon modes, five are Raman active, namely A_{1g}, E_g and $3T_{2g}$. The mode assignment of CZFMO shown in Fig. 5 is based on these predictions in accordance with the literature. The T-sites in the partial inverse spinel structure, such as $CoFe_2O_4$, are occupied by Fe^{3+} and partial Co^{2+}, depending on the inversion parameter. The observed Raman modes (E_g and T_{2g}), with frequencies below 600 cm^{-1} represent the bending of oxygen octahedra towards the metals in octahedral sites. The two high frequency modes $A_{1g}(1)$ and $A_{1g}(2)$ observed at 683 cm^{-1} and 617 cm^{-1} respectively, represent the symmetric stretching of surrounding oxygen with respect to metal ion on tetrahedral void (AO_4). The red shift of T_{2g}, E_g and A_{1g} modes indicates the incorporation of Zn and Mn in CFO lattice.

The deconvoluted Raman spectra for four major broad peaks at 136 cm^{-1}, 280 cm^{-1}, 522 cm^{-1} and 597 cm^{-1} for NBBT is shown in the top panel of Fig. 5. It can also be

seen that NBBT exhibits broad Raman bands due to the disorder in the sublattice A, the overlap of Raman modes caused by lattice anharmonicity, and also by the polycrystalline nature of the sample. All these features are comparable to the work reported for NBBT in literature [27-30]. NBBT with rhombohedral R3c phase exhibits a total of 13 Raman active modes, including $7A_1$ and 6E modes. At the same time, the coexistence of R and T (Pb4m, $3A_1+3B_1+2B_2+7E$) phases at MPB results in splitting of some A_1 modes. It was reported that NBT exhibits two broad Raman peaks around 130, 275 cm^{-1} and a doublet/triplet in the range 400-600 cm^{-1}. The presence of Ba at A-site of the lattice in NBBT results in the shift of peaks around 130 and 275 cm^{-1} towards lower wavelength [29]. Thus, the band at 130 cm^{-1} (A_1) can be assigned to Na-O and Ba-O lattice vibrations, dominant peak near 275 cm^{-1} (A_1) is due to the Ti-O vibrations and two peaks around 527 (E) and 597 cm^{-1} (A_1+E) are due to the rotation of oxygen octahedra as a superposition of transverse optical (TO) and longitudinal optical (LO) modes [27-29]. The weak Raman modes observed at high frequencies 742 and 843 cm^{-1} can be attributed to A_1(LO) and E(LO) modes arising due to the vibration of oxygen atoms [30]. The observation of Raman modes corresponding to NBBT and CZFMO for composites suggests the formation of two phase system with rhombohedral and cubic crystal structures. The broad nature of composite peaks indicates the superposition of modes from NBBT and CZFMO and no additional modes corresponding to intermediate phases can be seen. From Fig. 5 it is evident that with the increase of ferrite content, the intensity of all the peaks diminishes and modes become broader. When compared to the individual phases, composites show a red shift in A_1(TO4) modes representing the NBBT phase and blue shift in T_{2g}(2) mode of CZFMO with the increase in NBBT content. Thus, NBBT is strained compressively while the CZFMO experience a tensile strain.

The room temperature electrical resistivity (ρ) of NBBT sample is 7×10^{10} Ω-cm while for other composites it reduces by one order of magnitude. Resistivity of pure CZFMO is 4×10^{8} Ω-cm, which is of the same order of magnitude reported on this compound [31]. For 85:15, 75:25, 65:35 and 40:60 samples, the value of ρ decreases to 1×10^{10}, 6×10^{9} and 3×10^{9} and 8×10^{8} Ω-cm**.** The higher resistivity of the present compounds facilitated to pole them at higher electric fields (50-80 kV/cm). Fig. 6 shows the polarization-electric field hysteresis loops of NBBT and composites measured at room temperature. It can be seen that NBBT sample shows saturated ferroelectric polarization while the others show rounded corners of the hysteresis loop. For composites 85:15, 75:25 and 65:15 samples the polarization is dominated by the leakage current. The polarization maximum (and remnant polarization P_r) of NBBT, 85:15, 75:25, 65:35 and samples is 51 (37.5) μC/cm^2, 42 (32) μC/cm^2, 36 (31) μC/cm^2 29 (25) and 12.5 μC/cm^2 respectively. The P_r and coercivity (E_C=45 kV/cm) values of NBBT matches well with those reported in literature [17,32]. A trend of increasing E_C in the composites with the increase in ferrite concentration has been observed, which is possibly due to the pinning effect, caused by the oxygen vacancies (formed during sintering due to the presence of acceptor ions), that would hinder the reversal of spontaneous polarization of ferroelectric domains under an applied electric field [32]. The same trend is observed in the piezoelectric properties. Piezoelectric coefficient, d_{33}, of NBBT is 121 pC/N, which matches well with the reported value [33] while for the composites with 15, 25 and 35 mol. % ferrite it decreases to 78, 65 and 56 pC/N, respectively. Fig. 6 also presents S-E curve measured at 0.1 Hz for NBBT sample. The observation of butterfly-shaped curve under high voltages indicates the typical ferroelectric nature that is common for NBT-based materials. A maximum poling strain

of 0.19 % at 76 kV/cm is in the range reported in literature [34] and smaller than the reported by Dittmer et al.[35].

As the present composites with higher ferrite content exhibit large leakage, it is difficult to estimate ferroelectricity. We choose piezoresponse force microscopy (PFM) to study the inherent ferroelectric character at a nanoscale [36-38]. Scanning was performed in mirror polished, etched surfaces with roughness below 200 nm. Image contrast characterizes the out-of-plane piezoresponse (PR) for NBBT (Fig. 7) and 65:35 composite (Fig. 8). The topography image of pristine NBBT sample shows grains with 2 μm average size, where superimposed PR amplitude image (Fig. 7a) indicate the formation of bright and dark contrasts regions corresponding to positively and negatively polarized domains. In accordance with this, the phase image (Fig. 7b) shows striped type domains extending over several grains within the scanned region which have similarity to domains reported for NBT-type relaxor ferroelectrics [35]. For 65:35 composite and 40:60 sample (not shown) topography presents two different grains with smoother and coarser morphologies. From respective PR amplitude and phase images one can distinguish the spread of regions with zero polarization corresponding to ferrite phase delimited by ferroelectric ones. Within the NBBT grains one can observe the presence of several domains. The 65:35 sample exhibits a higher piezoresponse contrast signal compared to the 40:60 sample which was predictable from larger areas with zero PR. To observe the transformation of the FE domains, local poling experiments were conducted in electric contact mode with a scan speed of 0.5 Hz. Initially, 8 x 8 μm^2 square was poled with +20 $V_{d.c.}$ subsequent, within this region, a 4 x 4 μm^2 area was poled with -20 $V_{d.c.}$. An encompassing scan of 15 x 15 μm^2 area enable to observe the resulting OP PFM amplitude and phase presented in Fig. 8c and 8d. From contrast change observed in amplitude and phase PR, it is clear that the domains experienced a

reversal after poling; it is possible to observe that the width of the lithographed domains expands slightly after bias poling beyond the respective stimulated regions. Moreover, a noteworthy topological response can be traced to the positive bias lithographed area, confirmed by the spatial rearrangement of the phase contrast image. Although not presenting any PR contrast, these changes can be explained by the local irreversible displacement of NBBT grains that intricate the CZFMO grains present at the surface, that allows electric field propagation from the probe and attesting the ferroelectric nature the phase beneath. In addition, local piezoresponse hysteresis loops (Fig. 8 e) performed at random points of the composite surface shows the inherent ferroelectric response of the system. We observed local ferromagnetic nature of the CZFMO phase through magnetic force microscopy mode and the resulting image for 65:35 composite is shown in Fig. 9.

Fig. 10 (a) shows the magnetic hysteresis loops of ferrite and composite samples measured at room temperature. A soft ferromagnetic nature and a drop in magnetization values for composites with the increase in NBBT content indicate the dilution effect of ferromagnetic lattice with non-magnetic ones. The values of saturation magnetization (M_S) and coercivity (H_C) of CZFMO are 83 emu/g and 21 Oe as shown in the inset of Fig. 8 (a). The magnitude of M_S for composites was found to increase from 4.8 emu/g to 40.6 emu/g with the increase of ferrite content. At the same time the H_C of composites increased from 21 Oe to 43 Oe with the increase in NBBT content. It is normal in ME composites that homogenously dispersed lower fractions of magnetic component leads to the interrupted magnetic interaction between ferrite grains resulting in the increased coercivity [31].

Fig. 10 (b) shows the magnetization results of 65:35 composite samples before and after electrical poling. Virgin sample shows the M_S value of 18.9 emu/g whereas

after poling at 24 kV/cm and 47 kV/cm, it changes to 17.1 and 15.7 emu/g respectively. In other words, electrical poling influenced in a reduction of magnetization to about 18.5 % of its virgin state. In a recent work on CFO-NBBT composites, Pang et al.[39] observed a 14.6 % change in magnetization. Similarly, CFO-NBT composites exhibited a 15 % change in magnetization [40]. In two-phase composite samples of the present type, an electrically induced strain of ferroelectric phase due to converse piezoelectric effect is expected to induce a change in magnetization and coercivity of the magnetic phase. These stress induced changes in magnetic properties can be attributed to the change in magnetic anisotropy [41]. These features can be tracked to the changes observed in S-E curve (inset of Fig. 6), where it is evident that NBBT phase experiences a strain change of 0.07% at 24 kV/cm and 0.14 % at 47 kV/cm. In addition, the elongation experienced by the NBBT during the electrical poling process induces a compressive stress along poling direction and tensile stress along the magnetization direction in magnetic phase. The combined effects produce a negative magnetoelastic anisotropy, which creates hard axis along the poling direction and results in a reduction of M_S and M_r. These results are in conjunction with those reported for Ni/PMN-PT [41] and CFO-NBT [40] composites having negative magnetostrictive ferrimagnetic phases. We observed relatively smaller changes in M_S for 40:60 (9%) and 75:25 (12%) composites, which could be due to poor poling ability and lower volumes of magnetic phase. It is well reported that uniform distribution of magnetic phase inside of a ferroelectric phase is important to achieve optimum ME properties as the effective stress transfer is obtained from homogenously distributed grains of constituent phases [6]. From the results of SEM and PFM it is clear that 65:35 composite has homogenous distribution of grains corresponding to both the phases resulting in better ME coupling compared to remaining compositions of the series.

In order to verify the coupling between magnetic polarization and mechanical strain for the present composites, magnetostriction (λ) and piezomagnetic coefficient (q) were determined. Fig. 11 (a) shows in-plane parallel magnetostriction (λ_{11}) and in-plane perpendicular magnetostriction (λ_{12}) as a function of magnetic field for CZFMO and 65:35 composites. The piezomagnetic coefficient (q_{ij}) is derived for ferrite and composite samples by differentiating the magnetostriction parameter with respect to magnetic field ($q_{11}=d\lambda_{11}/dH$ and $q_{12}=d\lambda_{12}/dH$). The λ_{11} of CZFMO decreases with the increase in magnetic field and saturates at 1.5 kOe with a maximum value of -24 ppm. Similarly, the λ_{12} saturates at 1.1 kOe with a maximum value of 13 ppm. A similar behavior is observed for 65:35 composite (Fig. 11 b) with λ_{11}= -10.4 and λ_{12}=5.3 ppm with saturation fields of 1.7 and 1.2 kOe respectively. Inset of Fig. 11 presents the magnetic field dependence of q_{11} and q_{12} for CZFMO and 65:35 composite ceramics. The longitudinal piezomagnetic coefficient (q_{11}) shows maxima with a value of -0.023 ppm/Oe at H=0.3 kOe for CZFMO and -0.0087 ppm/Oe at 0.45 kOe for 65:35 composite. Similarly, transverse coefficient (q_{12}) shows a peak at H=0.5 kOe with a value of 0.044 ppm/Oe for CZFMO and 0.0114 ppm/Oe at H=0.8kOe for 65:35 composite. The position of peaks in q_{11} and q_{12} is an important factor in the design of high sensitivity magnetic field sensors as this corresponds to the field required to obtain maximum ME coefficient. In ME composites prepared with an undoped CFO, the piezomagnetic coefficient saturates at a field above 3 kOe [40,21] . The observed λ_{11} for CZFMO is reasonable in view of lower values reported in $Co_{0.6}Zn_{0.4}Fe_2O_4$ (17 ppm) [21] and $CoFe_{1.7}Mn_{0.3}O_4$ (120 ppm) [20, 37] . Gupta et al [22] in their work reported λ_{11}= 20 and λ_{12}=10 ppm for CZFMO. The disparity in these values can be attributed to the processing conditions. Undoped CFO exhibits saturated values of λ_{11} and λ_{12} in the range 150-250 and 90-150 ppm respectively depending on synthesis [19]. The observation

of smaller λ values for composite sample can be attributed to the contribution of change in the shape and stress induced magnetic anisotropy energy related to the inter coupling between the ferroelectric and magnetostrictive phases. The presence of non-magnetic grains embedded inside of a magnetic matrix brings the dilution effects which are normal in ME composites.

Fig. 12 shows the variation of direct magnetoelectric coupling coefficient (α) of 40:60, 65:35, 75:25 and 85:15 composites measured at 1 kHz under H_{ac}=1 Oe. ME coefficient initially increases with the magnetic field, shows a maxima around 1 kOe and decreases thereafter with further increase in magnetic field. This characteristic is related to the field dependence of magnetostriction shown in Fig. 11. The dependence of α on H tracks variation of the piezomagnetic coupling between piezoelectricity and magnetostriction. The increasing trend in α observed in the range 300-1.2 kOe is due to the growth of domains with favorable orientation to the field and further growth of domains above this field decreases the deformation leading to the drop in α. The ME coefficient observed at the maxima for 40:60, 65:35, 75:25 and 85:15 composites is 5.7, 8.2, 3.4 and 1.6 mV/cm-Oe, respectively. The observed values are relatively larger compared to CFO-NBT (0.5 mV/cm-Oe)[35], NBT-$NiFe_2O_4$ (0.155 mV/cm-Oe)[13]. As the ME effect is a product property between piezoelectricity and magnetostriction, the maximum ME coefficient depends on the volume fraction of CZFMO. With the increase in CZFMO content the value of α increases up to 35 mol. %, which can be attributed to the increase in magnetostrictively induced strain of composites with the volume fraction of ferrite phase. However, with further increase in ferrite, though the induced strain tends to increase, high concentration of the low resistance ferrite phase makes the samples difficult to polarize. This results in a low piezoelectric constant and

causes the charges developed in NBBT phase to leak through this low resistance phase path, to produce a lower ME response.

The compositional dependence of ME coefficient observed here can be related to the following explanation. For ME composites in off-resonance condition, the change in a is governed by the expression [14,43]

$$\alpha = (dE/dH)_{comp} = (dS/dH)_{comp}(dE/dS)_{comp}$$
$$= m_v (dS/dH)_{ferrite} (1 - m_v)(dE/dS)_{piezo} \quad \text{----- (1)}$$

Here m_v is the volume fraction of ferrite, dS/dH is change in strain with magnetic field, dE/dS is resulting electric field. After expanding the dE (=gdX) and dS (dX/C) in terms of mechanical and piezoelectric coefficients, Eq. (1) becomes

$$\alpha = m_v (dS/dH)_{ferrite} (1 - m_v)(g_{33} C_{33})_{piezo} \quad \text{---- (2)}$$

Here X is the stress, S is the strain, g_{33} is the piezoelectric voltage constant, and C_{33} is the stiffness constant. This relation (Eq. 2) indicates that optimized values of g_{33}, magnetization as well as λ are important to achieve ME output. The composite with 65:35 exhibit a g_{33}=4.1 x 10^{-3} V. m/N and M_S=18.9 emu/g which are optimum among the series and results in higher ME coefficient. 40:60 composite, inspite of higher magnetic properties suffer from large leakage behavior and can be poled partially resulting in poor d_{33} and g_{33}values. Hence, present composite system with improved resistivity (10^9 Ω-cm), lower H_C with reduced magnetic anisotropy have an advantage over CFO-piezoelectric based composites, because they can be operated at relatively lower magnetic fields.

4. Conclusions

Dense multiferroic CZFMO-NBT-BT lead-free composite were synthesized successfully. From the Raman spectroscopic studies, it was evident that the combination of two dissimilar materials could cause a strain in the participating phases of the composite resulting in the shift of Raman modes. NBBT and 85:15 composites exhibited saturated P-E hysteresis loops while the remaining samples suffer a large leakage current. From the local piezoresponse studies, we observed the domain reversal and intrinsic ferroelectricity of composites at a nanoscale. Magnetization measurements on electrically poled composites showed strong ME coupling due to converse piezoelectric effect. Direct ME measurements points to the fact that these lead-free composite materials have a strong ME reversal compared to other NBT-based composites studied in literature.

Acknowledgements

Authors would like to acknowledge the financial support from FCT, Portugal (SFRH/BPD/75582/2010).

References

1. H.Zheng, J.Wang, S.E.Lofland, Z.Ma, L.M.Ardabili, T.Zhao, L.S.Riba, S.R. Shinde, S.B.Ogale, F.Bai, D.Viehland, Y.Jia, D.G.Schlom, M.Wuttig, A.Roytburd, and R.Ramesh, *Science*, 2004, **303**, 661.
2. J.F.Scott, *J. Mater. Chem.*, 2012, **22**, 4567.
3. R.Ramesh and N. A. Spaldin, *Nat.Mater.*, 2007, **6**, 21.
4. J.M.Hu, Z.Li, J.Wang, and C.W.Nan, *J.Appl.Phys.*, 2010, **107**, 093912.

5. Y.H.Chu, L.W.Martin, M.B.Holcomb, M.Gajek, S.J.Han, Q.He, N.Balke, C.H. Yang, D.Lee, W.Hu, Q.Zhan, P.L.Yang, A.F.Rodriguez, A.Scholl, S.X.Wang, and R.Ramesh, *Nat.Mater.*, 2008, **7**, 478.
6. C.W.Nan, M.I.Bichurin, S.Dong, D.Viehland, and G.Srinivasan, *J.Appl.Phys.*, 2008, **103**, 031101.
7. M.Liu, O.Obi, J.Lou, Y.Chen, Z.Cai,S.Stoute, M.Espanol, M.Lew, X.Situ, K.S.Ziemer, V.G.Harris, and N.X.Sun, *Adv. Funct. Mater.*, 2009, **19**, 1826.
8. J.Das,M.Li, S.S.Kalarickal, S.Altmannshofer, K.S.Buchanan, J.F.Li, and D.Viehland, *Appl. Phys. Lett.*, 2010, **96**, 222508.
9. Z.Li, Y.Wang, Y.Lin, and C.W.Nan, *Phys. Rev. B*, 2009, **79**, 180406.
10. D.R.Patil and B.K.Chougule, *J.Alloy Compd.*, 2008, **458**, 335.
11. Y.Zhou, J.C.Zhang, L.Li, Y.L.Su, J.R.Cheng, and S.X.Cao, *J.Alloy Compd*., 2009, **484**, 535.
12. R.S. Devan, D R Dhakras, T G Vichare, A S Joshi, S R Jigajeni,Y.-R.Ma and B K Chougule, *J. Phys. D: Appl. Phys.*, 2008, **41**, 105010.
13. S.N.Babu, K.Srinivas, T.Bhima Sankaram, *J.Magn.Magn.Mater.*, 2009, **321**,3764.
14. S.C.Yang, C.W.Ahn, K.H.Cho, and S.Priya, *J. Am. Ceram. Soc.*, 2011, **94**, 3889.
15. Y.M.Chiang, G.W.Farrey , A.N.Soukhojak , *Appl. Phys. Lett.*, 1998, **73**, 3683.
16. B.J.Chu,D.R.Chen,G.RLi,Q.R.Yin., *J Eur.Ceram.Soc.*, 2002, **22**, 2115.
17. D.Maurya, Y.Zhou, Y.Yan and S.Priya, *J. Mater. Chem. C*, 2013, **1**, 2102.
18. M.Chen, Q.Xu, B.H.Kim, B.K.Ahn, J.H.Ko, W.J.Kang and O.J.Nam, *J. Eur. Ceram. Soc.*, 2008, **28**, 843.
19. K.K.Mohaideen and P. A. Joy, *Appl. Phys. Lett.*, 2012, **101**, 072405.
20. C.C.H.Lo, *IEEE Trans. Magn.*, 2007, **43**, 2367.
21. G.Srinivasan, E. T. Rasmussen, and R. Hayes, *Phys. Rev. B*, 2003, **67**, 014418.

22. A.Gupta, A.Huang, S.Shannigrahi, and R.Chatterjee, *Appl.Phys.Lett.*, 2011, **98**, 112901.

23. J.Teillet, F.Bourée, R.Krishnan, *J. Magn. Magn. Mater.*, 1993, **123**, 93.

24. G.O.Jones and P.A.Thomas, *Acta Crystallogr. B*, 2002, **58**, 168.

25. Z.Wang,R.T.Downs, V.Pischedda, R.Shetty, S.K.Saxena, C.S.Zha, Y.S.Zhao, D.Schifer and A.Waskowska, *Phys. Rev. B*, 2003, **68**, 094101.

26. P.Chandramohan,M.P.Srinivasan,S.Velmurugan, S.V.Narasimhan, *J. Solid State Chem.*, 2011, **184**, 89.

27. J.Kreisel, A.M.Glazer, G.Jones, P.A.Thomas, L.Abello and G.Lucazeau, *J. Phys.: Condens. Matter*, 2000, **12** , 3267.

28. L.Luo, W.Ge,J.Li, D.Viehland, C.Farley, R.Bodnar, Q.Zhang, and H.Luo, *J.Appl.Phys.*, 2011, **109**, 113507.

29. D.Rout, K.S.Moon, V.S.Rao and S.J.L.Kang, Study of the morphotropic phase boundary in the lead-free $Na_{1/2}Bi_{1/2}TiO_3$-$BaTiO_3$ system by Raman spectroscopy, *J.Ceram.Soc.Jap*., 2009, **117**, 797.

30. M.K.Niranjan, T.Karthik, S.Asthana, J.Pan, and U.V.Waghmare, *J.Appl.Phys.*, 2013, 113, 194106.

31. A.Gupta and R.Chatterjee, *J.Eur.Cer.Soc.*, 2013, **33**, 1017.

32. Q.Xu, M.Chen, W.Chen, H.Liu, B.H.Kim, B.K.Ahn, *Acta Mater.*, 2008, **56**, 642.

33. B.J.Chu, D.R.Chen, G.RLi and Q.R.Yin, *J.Eur.Ceram.Soc.*, 2002, **22**, 2115.

34. S.T.Zhang, A.B.Kounga, E.Aulbach, and Y.Deng, *J. Am. Ceram. Soc.*, 2008, **91**, 3950.

35. R.Dittmer, W.Jo, J.Rödel, S.Kalinin, and N.Balke, *Adv. Funct. Mater.*, 2012, **22**, 4208.

36. D.A. Bonnell, S.V. Kalinin, A.L.Kholkin, and A. Gruverman, *MRS Bull.*, 2009, **34**, 648.

37. E.V.Ramana, S.M.Yang, R.Jung, M.H.Jung, B.W.Lee, and C.U.Jung, *J.Appl.Phys.*, 2013, **113**, 187219.

38. E.V.Ramana, A.Mahajan, M.P.F.Graça, S.K.Mendiratta, J.M.Monteiro and M.A.Valente, *Mater. Res. Bull.*, 2013, **48**, 4395.

39. L.H.Pang, W.J.Ji, Y.Zhang, L.Wang, S.-T.Zhang, Z.-L.Luo and Y.-F.Chen, *J. Phys. D: Appl. Phys.*, 2009, **42**, 045304.

40. A. Srinivas, R.V.Krishnaiah, T.Karthik, P.Suresh, S.Asthana, and S.V.Kamat, *Appl. Phys. Lett.*, 2012, **101**, 082902.

41. T.Wu, A.Bur, K.Wong, J.L.Hockel, C.J.Hsu, H.K.D.Kim, K.L.Wang and G.P.Carman, *J.Appl.Phys.*, 2011, **109**, 07D732.

42. J.A.Paulsen, A.P.Ring, and C.C.H.Lo, J.E.Snyder and D.C.Jiles, *J.Appl.Phys.*,2005, 97, 044502.

43. J.V.Boomgaard and R.A.J.Born, *J. Mater. Sci.*, 1978, **13**, 1538.

Fig. 1 XRD patterns of sintered NBBT- CZFMO composites for CZFMO, 40:60, 65:35, 75:25, 85:15 and NBBT. Peaks corresponding to CZFMO and NBBT are shown as open circle and * symbols. Inset: (003)/(021) rhombohedral peak splitting of NBBT.

Fig. 2 Compositional dependence of lattice parameters of NBBT and CZFMO phases in composite samples.

Fig. 3 SEM images of NBBT – CZFMO composites for (a) CZFMO, (b) 65:35, (c) 85:15 and (d) NBBT.

Fig. 4 EDS mapping of 65:35 sample: (a) surface morphology, (b-e) EDS for Bi, Ti, Co, Fe and (f) mapping for all elements of composite.

Fig. 5 Raman spectra of NBBT, CZFMO and NBBT – CZFMO composites. Vertical continuous and dotted lines represent the modes corresponding to ferroelectric and ferrite phases of composites respectively.

Fig. 6 (a) P-E hysteresis loops for NBBT and composites with 85:15, 75:25 and 65:35 concentrations of ferroelectric and ferrite. Inset: S-E curve for NBBT sample.

Fig. 7 Out-of-plane piezoresponse images of NBBT sample. Topography superimpose with PR amplitude (a) and PR phase (b).

Fig. 8 PFM response of 65:35 composite: Topography superimposed with PR amplitude (a), PR phase (b) before lithography. Topography superimposed by PR amplitude (c) and PR phase (d) after performing bias lithography of +20 V over 8x8 μm^2 and -20 V over 4x4 μm^2 areas. (e) Piezoelectric hysteresis loops of NBBT, 65:35 and 40:60 composite samples.

Fig. 9: MFM image of CZFMO phase of 65:35 sample 5x5 μm^2 : (a) topography and (b) phase.

Fig. 10 (a) Magnetic hysteresis loops of 40:60, 65:35, 75:25 and 85:15 NBBT–CZFMO composites. Inset: M-H curve for CZFMO. (b) Magnetic hysteresis loops of 65:35 composite samples before and after electrical poling.

Fig. 11 Room temperature longitudinal and transverse magnetostriction of CZFMO and 65:35 composite samples. Magnetic field dependence of piezomagnetic coefficients are shown in inset of (a) and (b) respectively for CZFMO and 65:35.

Fig. 12 Magnetoelectric coefficient verses magnetic field curves for 40:60, 65:35, 75:25 and 85:15 composites measured at an ac magnetic field of 1 Oe.

.

Fig.1

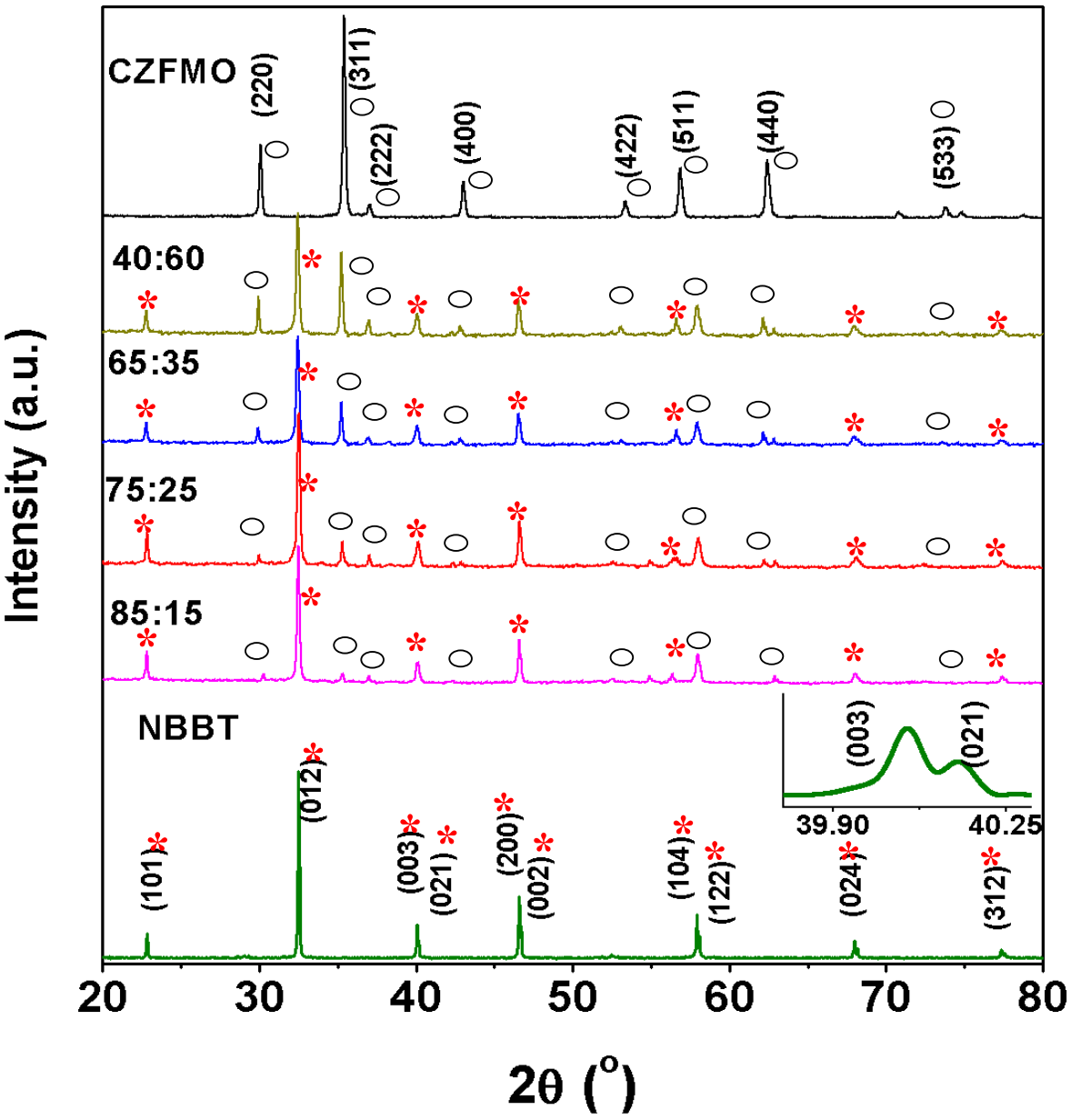

Fig.2

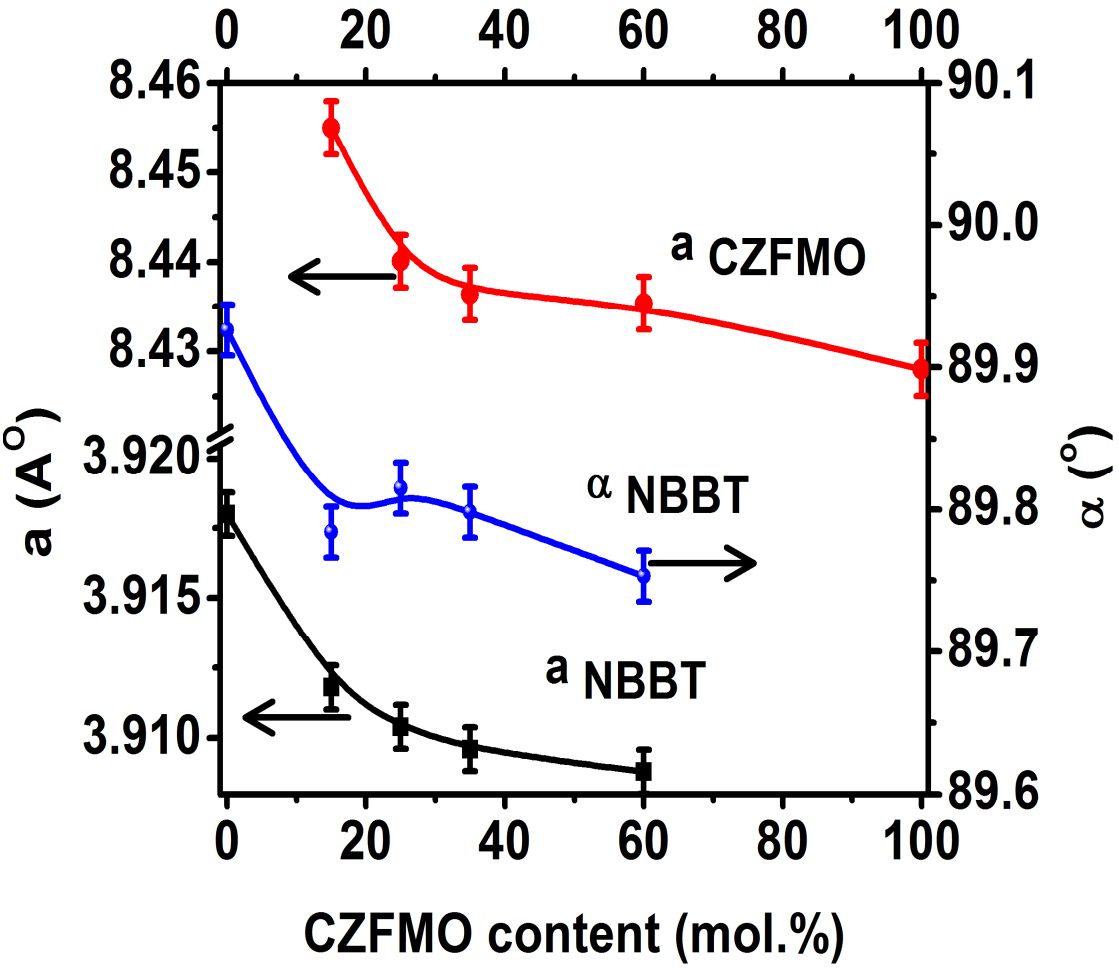

Fig.3

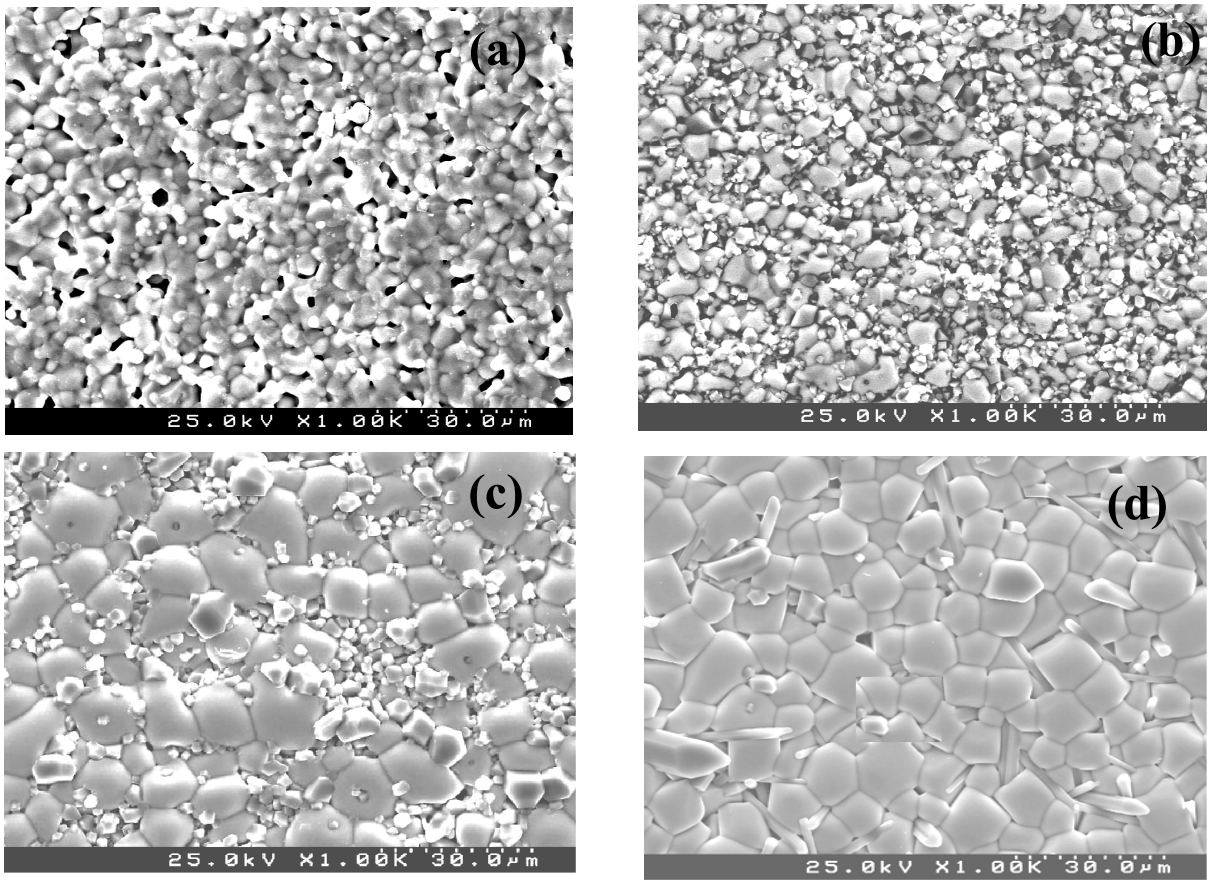

Fig.4

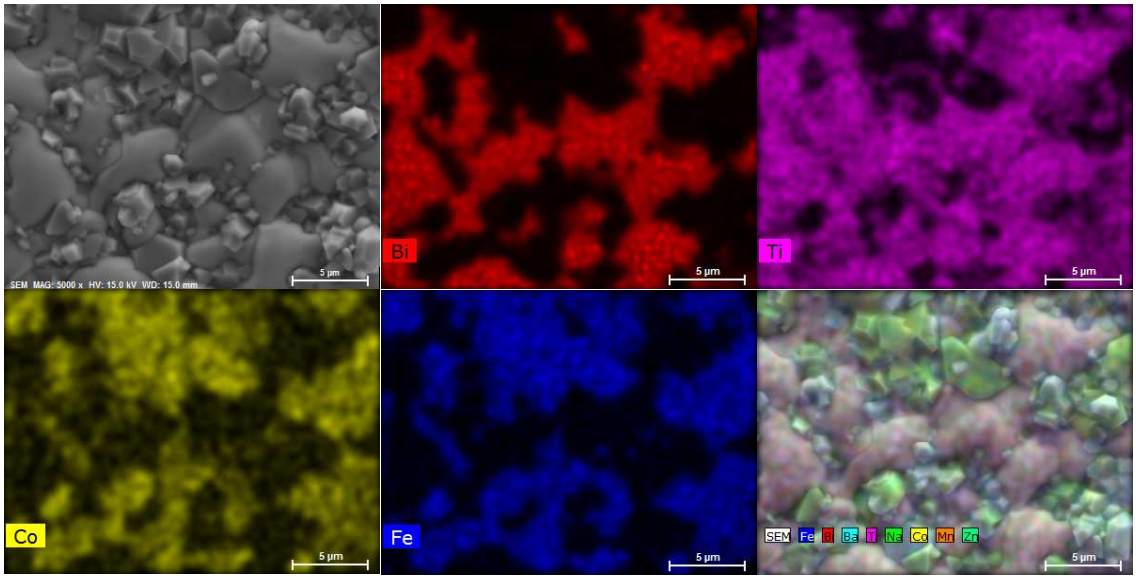

Fig.5

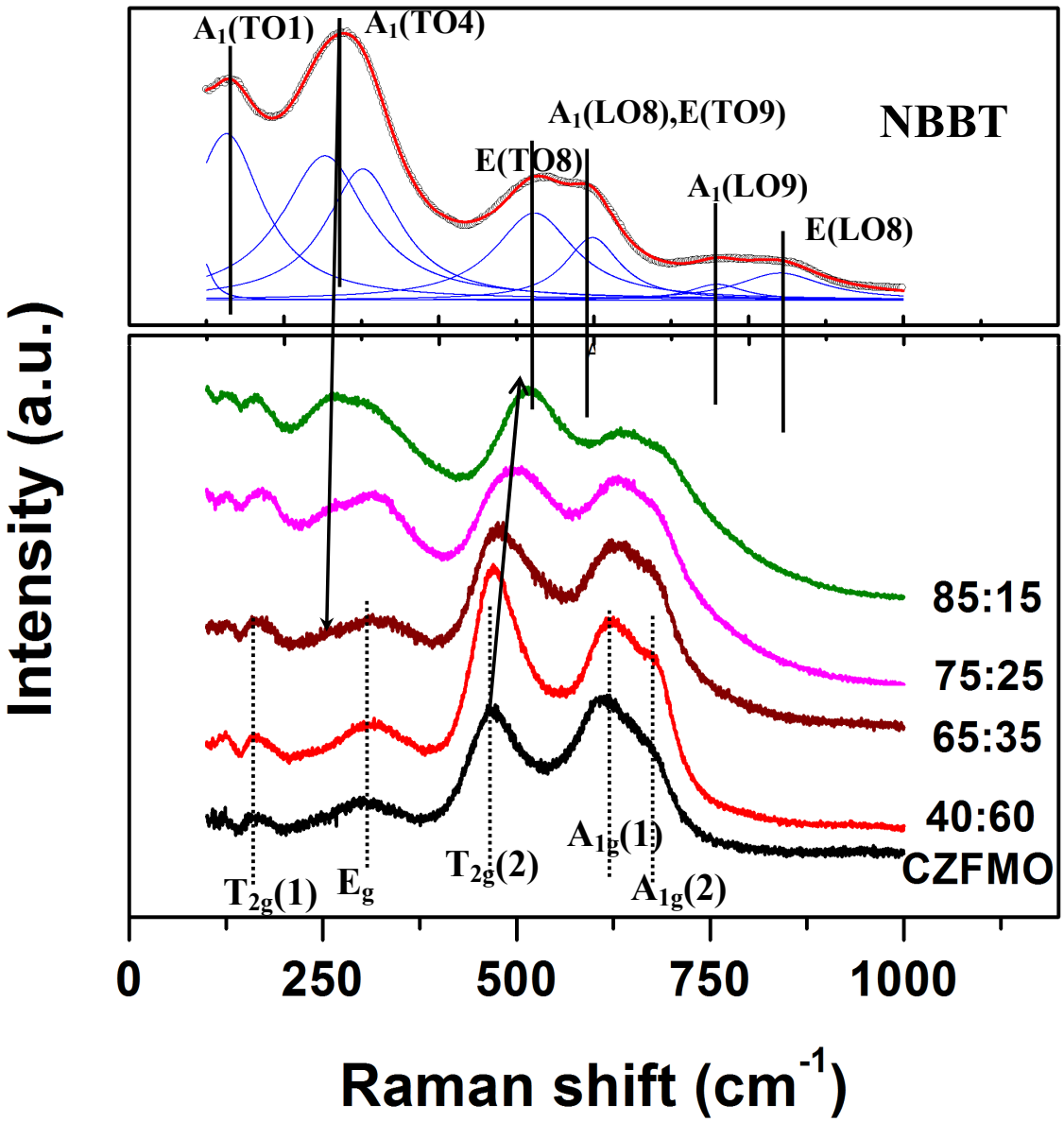

Fig.6

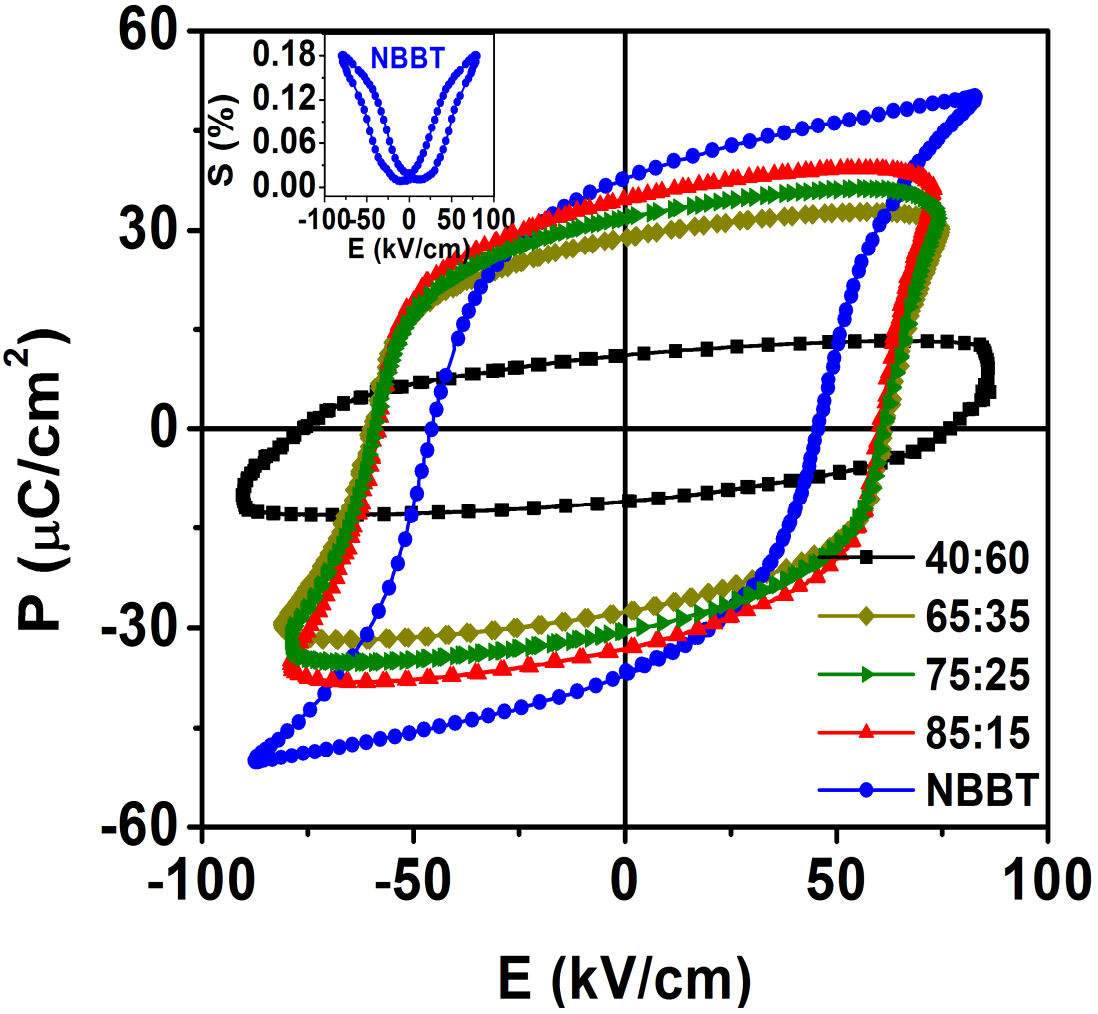

Fig.7

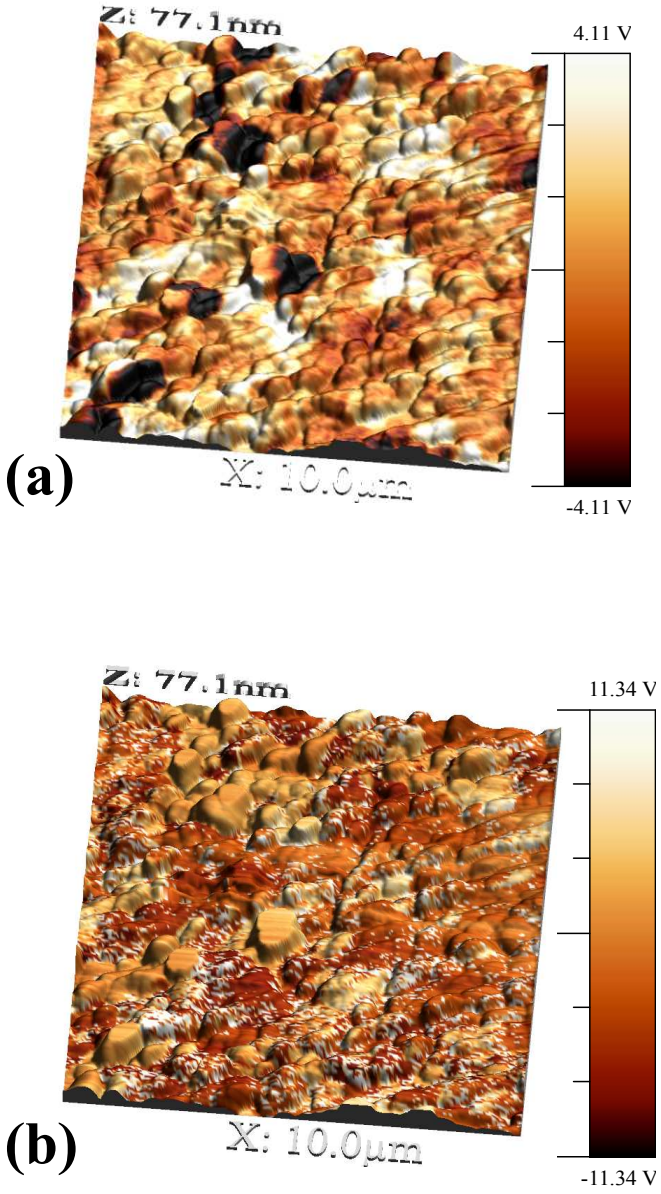

Fig.8

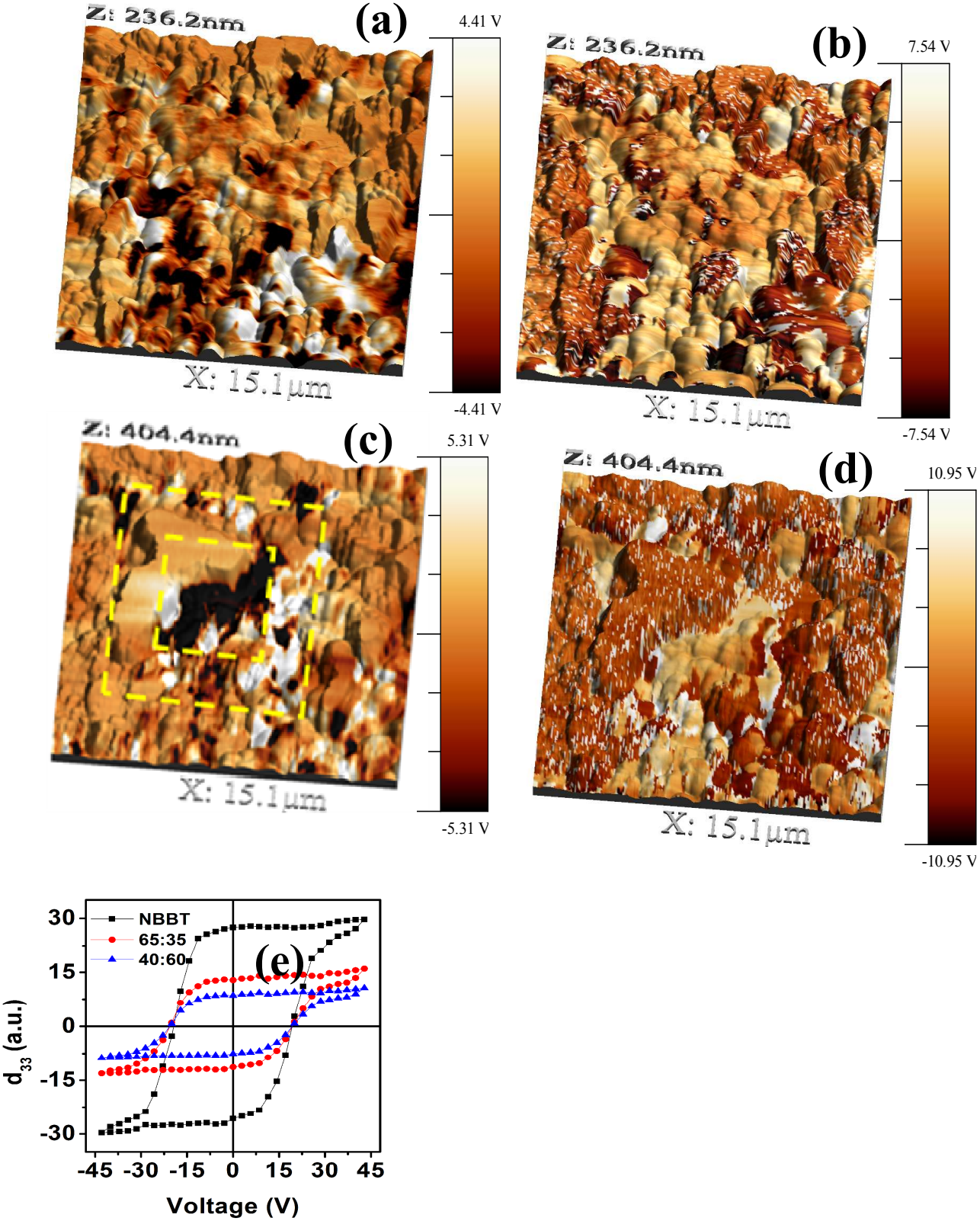

Fig.9

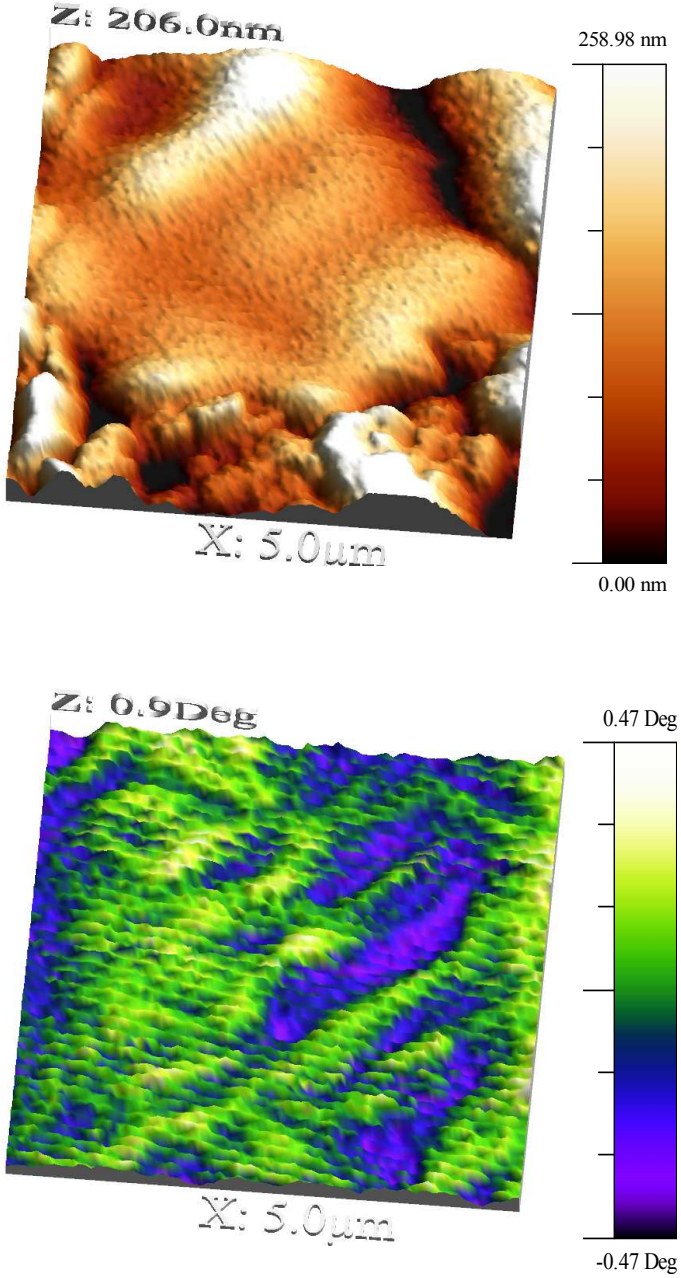

Fig.10

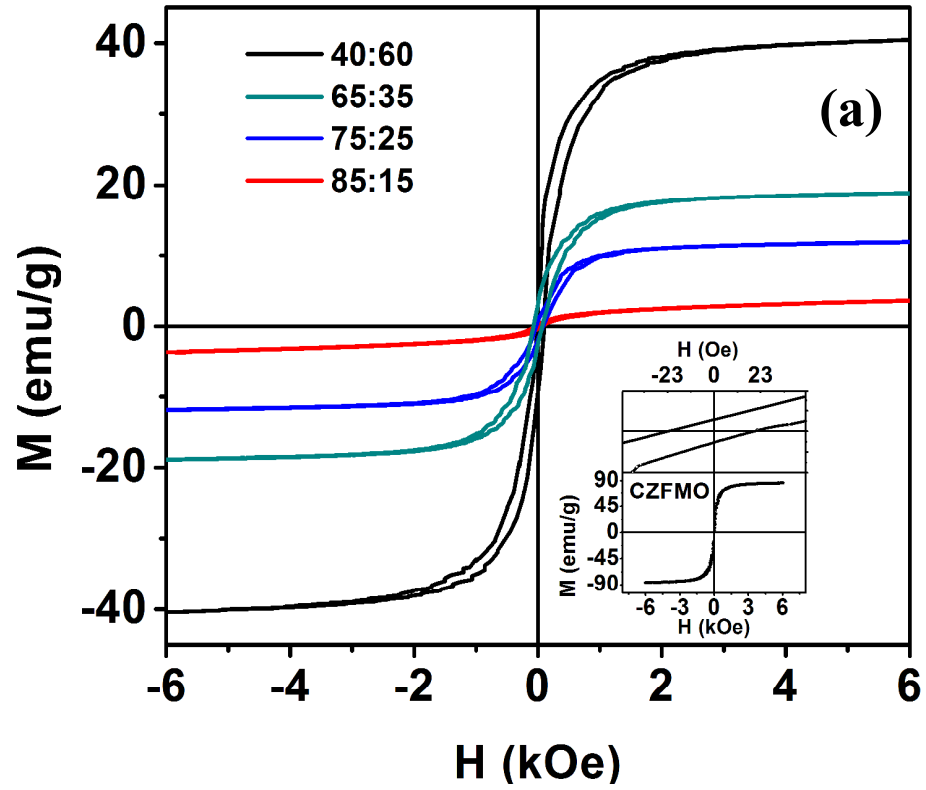

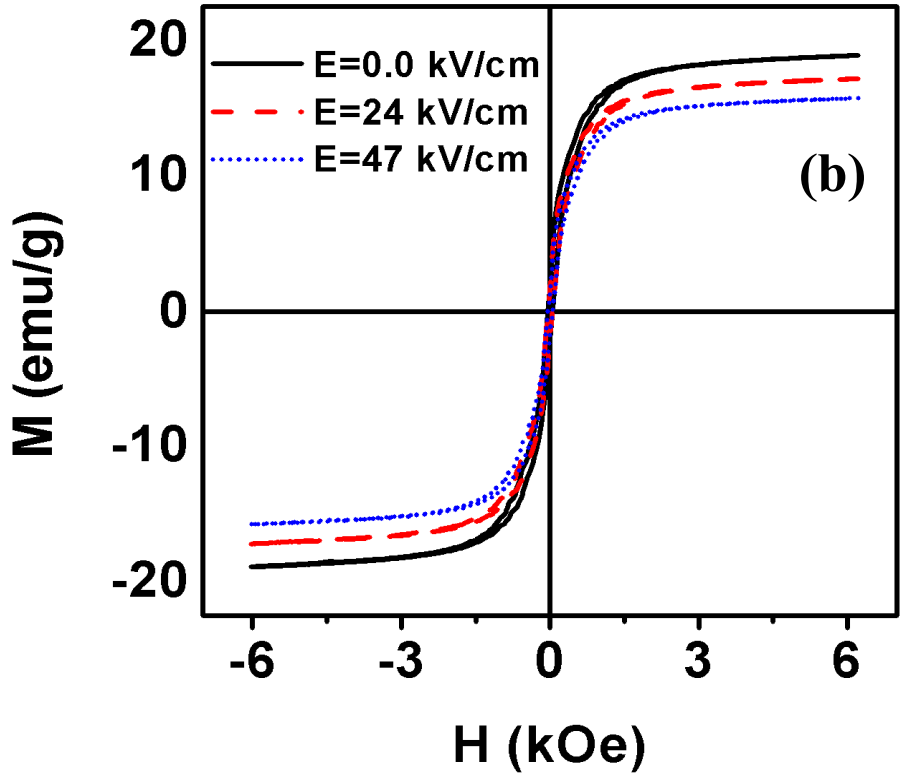

Fig.11

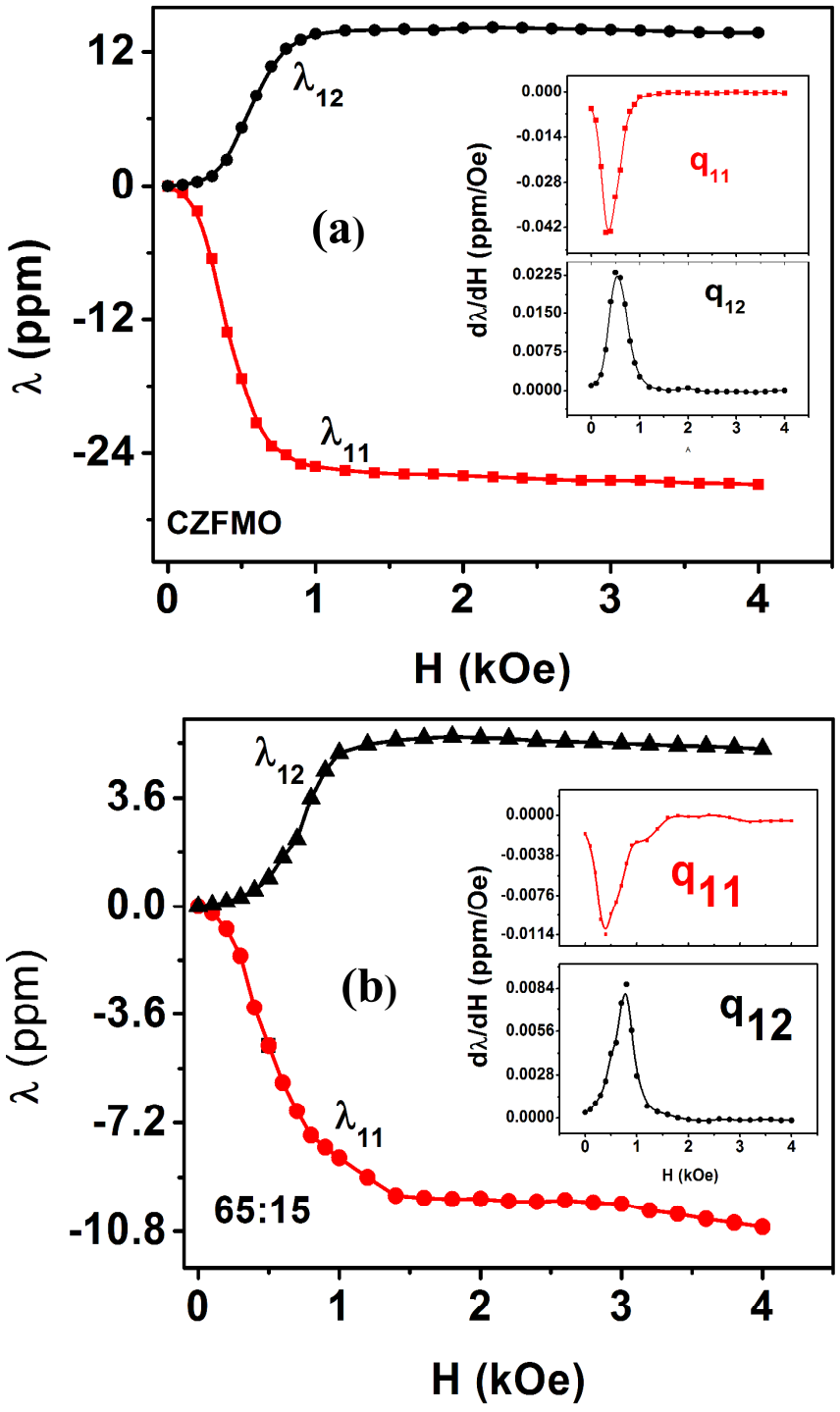

Fig.12